

# Single Cells Are Spatial Tokens: Transformers for Spatial Transcriptomic Data Imputation

Hongzhi Wen

Michigan State University  
wenhongz@msu.edu

Jiayuan Ding

Michigan State University  
dingjia5@msu.edu

Yuying Xie

Michigan State University  
xyy@msu.edu

Wenzhuo Tang

Michigan State University  
tangwen2@msu.edu

Renming Liu

Michigan State University  
liurenmi@msu.edu

Wei Jin

Michigan State University  
jinwei2@msu.edu

Feng Shi

TigerGraph, Inc.  
bill.shi@tigergraph.com

Jiliang Tang

Michigan State University  
tangjili@msu.edu

## ABSTRACT

Spatially resolved transcriptomics brings exciting breakthroughs to single-cell analysis by providing physical locations along with gene expression. However, as a cost of the extremely high spatial resolution, the cellular level spatial transcriptomic data suffer significantly from missing values. While a standard solution is to perform imputation on the missing values, most existing methods either overlook spatial information or only incorporate localized spatial context without the ability to capture long-range spatial information. Using multi-head self-attention mechanisms and positional encoding, transformer models can readily grasp the relationship between tokens and encode location information. In this paper, by treating single cells as spatial tokens, we study how to leverage transformers to facilitate spatial transcriptomics imputation. In particular, investigate the following two key questions: (1) *how to encode spatial information of cells in transformers*, and (2) *how to train a transformer for transcriptomic imputation*. By answering these two questions, we present a transformer-based imputation framework, SpaFormer, for cellular-level spatial transcriptomic data. Extensive experiments demonstrate that SpaFormer outperforms existing state-of-the-art imputation algorithms on three large-scale datasets.

## KEYWORDS

single-cell analysis, spatial transcriptomics, transformers

### ACM Reference Format:

Hongzhi Wen, Wenzhuo Tang, Wei Jin, Jiayuan Ding, Renming Liu, Feng Shi, Yuying Xie, and Jiliang Tang. 2023. Single Cells Are Spatial Tokens: Transformers for Spatial Transcriptomic Data Imputation. In *Proceedings of ACM Conference (Conference'17)*. ACM, New York, NY, USA, 12 pages. <https://doi.org/10.1145/nnnnnnnnnnnnnnnn>

Permission to make digital or hard copies of all or part of this work for personal or classroom use is granted without fee provided that copies are not made or distributed for profit or commercial advantage and that copies bear this notice and the full citation on the first page. Copyrights for components of this work owned by others than ACM must be honored. Abstracting with credit is permitted. To copy otherwise, or republish, to post on servers or to redistribute to lists, requires prior specific permission and/or a fee. Request permissions from [permissions@acm.org](mailto:permissions@acm.org).

*Conference'17, July 2017, Washington, DC, USA*

© 2023 Association for Computing Machinery.  
ACM ISBN 978-x-xxxx-xxxx-x/YY/MM...\$15.00  
<https://doi.org/10.1145/nnnnnnnnnnnnnnnn>

## 1 INTRODUCTION

Spatial transcriptomic technologies [3, 12, 24, 35, 40, 53, 55, 65, 78] have rapidly developed in recent years and emerged as next-generation tools for biomedical research. They produce detailed single-cell transcriptomic profiles along with the location of cells within a tissue, yielding deeper insights into cell identity and functionality than ever. These technologies vary in their technical parameters and typically involve a trade-off among spatial resolution, the number of genes profiled, and accuracy. For instance, *situ* hybridization (ISH) based methods [12, 50, 54] can achieve the highest subcellular spatial resolution. However, as the number of profiled genes increases, the requirement for additional rounds of hybridization also increases, which elevates the potential for cumulative errors [85]. As a result of these trade-offs, spatial transcriptomic data generally suffer from low mRNA capture efficiency. In other words, spatial transcriptomics profiling may miss a significant number of expressed genes, thereby resulting in many false zero counts in observed gene expression data.

An effective approach to mitigate this problem is applying imputation methods to rectify the false zeros. There are numerous types of imputation methods for *conventional transcriptomic data*, including generative probability models [20, 31], matrix factorization [36, 43, 72, 75] and deep learning models [18, 25, 58, 62, 71, 80]. Nevertheless, the majority of these methods tend to yield suboptimal performance when performing imputation for spatial transcriptomic data, as they do not leverage the presented spatial information. Notably, the spatial locations of cells provide important information about cell-cell interactions as well as cell similarities [7, 41, 52, 67, 84], which have the great potential to advance the imputation process. Specifically, the location of cells determines the microenvironment where they are impacted by both direct signals from neighboring cells [7] and soluble signals within the tissue. This can significantly affect the evolution of the cells. First, the location of cells can provide insights into the potential effects that cells receive from their neighboring cells. Second, cells that are spatially closer to each other are more likely to experience more similar microenvironments and exhibit greater gene expression correlation compared to more distant cells. Hence, it is of high importance to leverage such spatial information for data imputation.

To effectively utilize spatial information, graph neural networks have been recently utilized for spatial transcriptomic analysis [42, 82]. Concretely, graph neural networks (GNNs) are applied on the cell-cell neighboring graphs built on the spatial positions, which only connect the adjacent cells in spatial location. Therefore, these methods are limited to model a localized spatial context, which can be unfavorable for identifying long-range correlated cells. For example, Treg cells are scarce spatially in many tissues but still tend to be homologous and share similar gene expression profiles [67]. Hence, it is desirable to capture the cell interactions from broader contexts. To achieve this goal, we employ the transformer model [76] for the studied problem. The transformer model was originally designed for textual data. It uses multi-head self-attention mechanisms to model relationships between input tokens and utilizes positional encoding to model the locations of tokens. Transformers are able to weigh the importance of each input token relative to all other tokens, rather than adjacent ones as in GNNs. In our studied problem, by treating cells as tokens, we can readily apply the transformer model to capture long-range correlations between cells. Furthermore, transformers have great potential in improving imputation by identifying intracellular signaling pathways, as they have already demonstrated their exceptional capability in uncovering the intricate relations between tokens in various domains [28, 63].

In this paper, we investigate two key questions when applying transformers to spatial transcriptomic imputation: (1) *how to encode spatial information of cells in transformers*, and (2) *how to train a transformer for transcriptomic imputation*. To answer the first question, the natural idea is to adopt the positional encodings from common transformers [22, 76] to encode spatial cellular coordinates. However, the spatial coordinates of cells are continuous and irregular, which are essentially different from the discrete coordinates in the common practice of transformers. Therefore, efforts are still desired to design positional encodings for spatial transcriptomics. To address this issue, we investigate existing positional encodings, compare their advantages and disadvantages, and conduct comprehensive experiments to obtain a best practice for spatial transcriptomics. To answer the second question, we generalize the well-studied imputation models for conventional transcriptomic data into a flexible autoencoder framework, where we adopt a transformer as the encoder. Furthermore, we propose a new bi-level masking technique that can be plugged into the general autoencoder framework. With the solutions to two questions, our proposed framework, SpaFormer, consistently achieves outstanding imputation performance on three large-scale cellular level spatial transcriptomic datasets.

## 2 PRELIMINARY

### 2.1 Problem Statement

Before we introduce the problem statement, we first introduce some notations and basic concepts. A typical spatial transcriptomic dataset is comprised of two essential components, i.e., the gene expression of cells and the corresponding spatial locations. It is important to note that the focus of this paper is on high-resolution cellular-level datasets (typically generated by ISH-based techniques), as opposed to the commonly studied spot-level datasets (e.g., Seq-based data) present in most published works [21, 34, 42, 44]. We denote

the gene expression data as a matrix  $X \in \mathcal{R}^{N \times k}$ , where  $N$  is the number of cells, and  $k$  is the number of genes. Hereby,  $X_{i,j}$  denotes the count of the  $j$ -th gene captured in the  $i$ -th cell. We use  $C \in \mathcal{R}^{N \times 2}$  to denote the two-dimensional coordinates of each cell, where those coordinates are based on the center position of each cell. Note that each dataset is composed of multiple field-of-views (FOVs). Each FOV contains thousands of cells and might not be adjacent to each other. Thus, we focus on units of FOVs by default.

In the spatial transcriptomic imputation problem, we suppose that a part of the input values in  $X$  are missing, denoted as a mask matrix  $M \in \{0, 1\}^{N \times k}$ , where the value of  $X_{i,j}$  can only be observed when  $M_{i,j} = 1$ . A partially observed data matrix  $\tilde{X}$  is defined as:

$$\tilde{X}_{i,j} = \begin{cases} 0 & M_{i,j} = 0 \\ X_{i,j} & M_{i,j} = 1 \end{cases} \quad (1)$$

Our objective is to predict the missing values  $X_{i,j}$  at  $M_{i,j} = 0$ , given the partially observed data  $\tilde{X}_{i,j}$  and the spatial positions  $C$ . Note that in this work, we treat cells as tokens thus we will use these two terms exchangeably in the remaining of the paper.

### 2.2 Transformers

An essential component of our SpaFormer framework is transformer encoders. Transformers are originally designed for natural language processing tasks and later adopted to many other domains [1, 22, 46], achieving tremendous success. The original transformer comes with an encoder-decoder architecture, while in this paper we only take advantage of a transformer encoder. Specifically, a transformer encoder [76] consists of alternating layers of Multi-head Self-Attention (MSA) and Multi-Layer Perceptron (MLP) blocks. Prior to each block, Layer Normalization (LN) is performed, and a residual connection is established following every block. To be concrete, a transformer encoder can be formulated as:

$$H_0 = [x_1 E; x_2 E; \dots; x_n E] + E_{\text{pos}}, \quad E \in \mathcal{R}^{k \times d}, E_{\text{pos}} \in \mathcal{R}^{n \times d} \quad (2)$$

$$H'_\ell = \text{MSA}(\text{LN}(H_{\ell-1})) + H_{\ell-1}, \quad \ell = 1 \dots L \quad (3)$$

$$H_\ell = \text{MLP}(\text{LN}(H'_\ell)) + H'_\ell, \quad \ell = 1 \dots L \quad (4)$$

where  $x_i$  is  $i$ -th input token, i.e.,  $i$ -th cell in an FOV,  $H_\ell \in \mathcal{R}^{n \times d}$  is the embeddings of tokens in the  $\ell$ -th layer,  $n$  is the number of the input cells,  $d$  is the hidden dimension,  $E$  is a learnable transformation layer,  $E_{\text{pos}}$  is positional encodings for each cell. In our cases, positional encodings mainly encode the spatial positions, which is detailed in Section 3. To demonstrate MSA, we first introduce Self-Attention (SA). In a regular transformer, SA uses dot-product attention to map input queries ( $Q$ ), keys ( $K$ ), and values ( $V$ ), creating encoded representations for each unit. Specifically,

$$\text{Attention}(Q, K, V) = \text{softmax} \left( \frac{QK^\top}{\sqrt{d_h}} \right) V \quad (5)$$

where query  $Q$ , key  $K$ , and value  $V$  are projected from the same embedding matrix  $H_\ell$  (from Eq. 4) with different learned projection matrices,  $d_h$  is the hidden dimension size which is used as a scaling factor. On top of that, MSA extends SA where we conduct  $k$  SA in

parallel and project their concatenated outputs, formulated as:

$$\text{MSA}(\mathbf{H}_\ell) = [\text{head}_1; \text{head}_2; \dots; \text{head}_h] \mathbf{W}^O \quad (6)$$

$$\text{head}_i = \text{Attention} \left( \mathbf{H}_\ell \mathbf{W}_i^Q, \mathbf{H}_\ell \mathbf{W}_i^K, \mathbf{H}_\ell \mathbf{W}_i^V \right) \quad (7)$$

where the projections matrices for each head  $\mathbf{W}_i^Q \in \mathbb{R}^{d \times d_h}$ ,  $\mathbf{W}_i^K \in \mathbb{R}^{d \times d_h}$ ,  $\mathbf{W}_i^V \in \mathbb{R}^{d \times d_h}$ , and  $\mathbf{W}_i^O \in \mathbb{R}^{d \times d}$  are learnable parameters.

In our implementation, we adopt Performer [15], an efficient variant of transformers. Performer proposed high-efficient kernelized attention to approximate the original attention in Eq. 5. As a result, Performer reduces the time complexity of transformers from quadratic to linear w.r.t number of input tokens, so that they can be applied to thousands of cell tokens within each FOV. In the following sections, we will first introduce how to capture spatial information as positional embedding in transformers and then detail the proposed framework.

### 3 ENCODING SPATIAL INFORMATION IN TRANSFORMERS

When employing transformer models to spatial transcriptomic data, a critical challenge is how to encode spatial information in transformers. In a standard transformer, positional encodings are added to the token embeddings to make use of the positional information of tokens. Thus, it paves us a way to capture spatial transcriptomics by producing positional encoding for every single cell. However, the coordinates of spatial transcriptomics are continuous and irregular, which are essentially different from the sequential or image data. To tackle this issue, we investigate three general groups of positional encodings and demonstrate how we apply them to spatial transcriptomics, namely patch-based, coordinate-based, and graph-based positional encodings. These positional encodings can be directly added to cell embeddings. On top of that, we discuss potential limitations of these positional encodings and thus introduce two more advanced model-based positional encodings.

#### 3.1 Patch-based Positional Encodings

We define patch-based positional encodings as encodings derived from discrete and regular patches. For example, ViT [22] separates an image into  $16 \times 16$  patches, so that patches lie in a regular grid. Positional encodings generated from these patch coordinates are considered patch-based positional encodings. This kind of positional encoding have been widely applied in computer vision such as ViT [22], DeiT [73], and FPT [88]. To apply this approach to spatial transcriptomic data, we segment a whole input region, a.k.a, a field-of-view (FOV), into regular patches. Note that this will result in identical positional encodings for cells located in the same patch. Smaller patch size will improve the resolution and accuracy of positional encodings, but also burden the generalization ability and scalability of the model. Therefore, it is important to select an appropriate patch size. In this paper, we first pad and rescale each FOV to a unified square shape, then segment each FOV into  $100 \times 100$  patches, where each patch contains 0.3-0.55 cell on average due to the distinct cell size of different tissues. We denote patch coordinates as  $(x, y) \in [0, 99] \times [0, 99]$ . Based on the patch coordinates, there are generally two ways to produce positional encodings (PE) for each patch.

**Learnable PE**, which is introduced in ViT [22], where it independently learns a positional encoding for each individual position. This is equivalent to creating a learnable lookup table  $\mathbf{P} \in \mathbb{R}^{100 \times 100 \times d}$ , where  $\mathbf{P}_{x,y,:}$  is the  $d$  dimensional positional encoding for patch  $(x, y)$ .

**Sinusoid PE**, which is proposed in vanilla transformer [76]. The original version is designed for sequential data, while we can extend it to 2-dimensional space similar to DETR [10] and Mi2LaTeX [83]. Specifically, we formulate the 2-dimensional sinusoid PE as:

$$\text{PE}(x, y, 2i) = \sin \left( x / 10000^{4i/d} \right) \quad (8)$$

$$\text{PE}(x, y, 2i + 1) = \cos \left( x / 10000^{4i/d} \right) \quad (9)$$

$$\text{PE}(x, y, 2j + d/2) = \sin \left( y / 10000^{4j/d} \right) \quad (10)$$

$$\text{PE}(x, y, 2j + 1 + d/2) = \cos \left( y / 10000^{4j/d} \right) \quad (11)$$

where  $i, j \in [0, d/4)$  specify the feature dimensions.

#### 3.2 Coordinate-based Positional Encodings

Coordinate-based positional encodings aim to generate positional encodings directly from the continuous spatial coordinates. In order to improve the generalizability, we first normalize the spatial coordinates  $\mathbf{C} \in \mathbb{R}^{n \times 2}$  to  $[0, 1]$  by applying min-max normalization in each FOV. The normalized coordinates are denoted as  $\tilde{\mathbf{C}}$ . Next, we discuss two ways to generate positional encodings:

**Naive PE**, which projects spatial coordinates  $\tilde{\mathbf{C}}$  to desired dimension  $d$  via a linear transformation or MLP. For example,

$$\mathbf{P} = \sigma \left( \tilde{\mathbf{C}} \mathbf{W} + \mathbf{b} \right) \quad (12)$$

where  $\mathbf{W} \in \mathbb{R}^{2 \times d}$  and  $\mathbf{b} \in \mathbb{R}^d$  are learnable parameters,  $\sigma$  is a non-linear function, and  $\mathbf{P} \in \mathbb{R}^{n \times d}$  is the positional encodings. Compared to learnable PE in Section 3.1, naive PE imposes the ordinal relation between coordinates. Furthermore, it does not depend on predefined patches, thus the positional encodings can be adapted to a better resolution.

**Sinusoid PE**, which is the same as Eq. 8, Eq. 9, Eq. 10 and Eq. 11, except that discrete patch coordinates  $x$  and  $y$  are replaced with continuous cell coordinates  $\tilde{\mathbf{C}}_{:,0}$  and  $\tilde{\mathbf{C}}_{:,1}$ . Note that the frequency of the sinusoidal functions needs to be changed to accommodate the scale of the coordinates.

#### 3.3 Graph-based Positional Encodings

Graph-based positional encodings are derived from the spatial adjacency graph that connects adjacent tokens. Graph-based positional encodings are popular in some specific domains where graphs are considered as a natural way to represent spatial interaction, e.g. traffic flow [87], and molecules [61]. The motivation of graph-based positional encodings is that the spatial adjacency graph conveys the relative position relations between tokens so that we can capture the positional information by encoding the spatial adjacency graph. To this end, we construct a spatial graph in which cell pairs are connected when the euclidean distance is smaller than  $15\text{-}25\mu\text{m}$ . As a result, each cell is connected to 4-6 cells on average, depending on the specific tissue type. The resulting adjacency matrix is denoted

	Sources	Distance Aware.	Global Effec.	Translation Invari.	Structure Aware.	Other Issues
Sinusoid PE	Patch / Coordinate	✓	✓	✗	✗	
Learnable PE	Patch	✓	✓	✗	✗	
Naive PE	Coordinate	✓	✓	✗	✗	
RWPE	Graph	✗	✗	✓	✓	
LapPE	Graph	✓	✓	✓	✓	
Relative PE	Distance	✓	✓	✓	✗	Sign Ambiguity Scalability
SignNet [45]	Model	✓	✓	✓	✓	
Cond PE	Model	✓	✗	✓	✓	

Table 1: Comparison between positional encodings regarding the desired properties for spatial transcriptomics.

as A. Next, we present two ways to encode positional information from spatial adjacency graphs:

**Random Walk PE**, which is proposed in LSPE [23], defined as:

$$p_i^{\text{RWPE}} = \left[ \text{RW}_{ii}, \text{RW}_{ii}^2, \dots, \text{RW}_{ii}^k \right] \in \mathbb{R}^k,$$

where  $\text{RW} = \text{AD}^{-1}$  is the random walk operator,  $\text{D}$  is the degree matrix, and  $k$  is the number of random walk steps. This positional encoding is effective in encoding graph structures [11, 23]. However, it should be noted that the random walk positional encoding (RWPE) hardly encodes distance information. Furthermore, it is limited to structural information within the  $k$ -th order neighborhood and thus overlooks the global context.

**Laplacian PE**, which is to use Laplacian eigenvectors [5] as positional encodings. Specifically, graph Laplacian  $\text{L}$  is defined as  $\text{L} = \text{I}_n - \text{D}^{-1/2} \text{AD}^{-1/2} = \text{U} \Lambda \text{U}^T$ , where  $\text{I}_n$  is an identity matrix, and  $\Lambda \in \mathcal{R}^{k \times k}$  and  $\text{U} \in \mathcal{R}^{n \times k}$  correspond to the eigenvalues and eigenvectors respectively,  $n$  is the number of nodes, and  $k$  is the number of top eigenvalues we select. The Laplacian eigenvectors constitute a local coordinate system that retains the overall structure of the graph [23]. Thus, we can use the  $i$ -th row of eigenvector matrix  $\text{U}$  as the positional encoding for node  $i$  in the graph, a.k.a. a cell  $i$ . Laplacian positional encoding (LapPE) is generally a good choice despite being limited by sign ambiguity [39]. A straightforward approach to address this problem is to randomly flip the sign of eigenvectors during training, to force the model to be sign-invariant.

### 3.4 Model-based Positional Encodings

Despite that the aforementioned positional encodings can encode spatial information, each of them has certain limitations. Specifically, patch-based and coordinate-based positional encodings, such as sinusoid PE, learnable PE, and naive PE, are dependent on the absolute location, however, studies have shown that relative positional encodings [51, 86], which consider the pair-wise relationships, generally perform better in various domains [47, 68]. One key advantage of relative positional encodings is their translation-invariant property. Translation-invariance refers to the property that positional encodings remain unchanged upon global translation of the coordinates, thereby enhancing the generalizability of transformers. However, relative positional encodings are generally not scalable because they cannot accommodate recent efficient transformers [14, 60, 81]. These efficient transformers achieve linear time complexity w.r.t the number of input tokens, which is highly demanded in processing thousands of cells as input tokens.

Therefore, we cannot directly adopt relative positional encoding in our SpaFormer framework.

Fortunately, graph-based positional encodings also achieve translation invariance since they are derived from the spatial adjacency graph, which is naturally based on invariant pair-wise distances. Nevertheless, RWPE cannot accurately encode pair-wise distance, while LapPE suffers from sign ambiguity. Therefore we introduce two advanced models to generate positional encodings based on spatial adjacency graphs.

**SignNet** [45] proposes a sign invariant and permutation invariant network to learn positional encodings from the Laplacian eigenvectors of a target graph. The resulting positional encodings inherit the advantages of LapPE while not suffering from sign ambiguity.

**Cond PE**, which stands for conditional positional encodings, originally proposed in CPVT [16]. In the original version, CPVT added a simple convolution layer before vision transformers, to provide positions conditioned on the local neighborhood of each input token. We adopt this idea while substituting the visual convolution with a graph convolution, as it is more feasible to implement the graph convolution on a spatial graph compared to directly convolute the sparsely positioned cell tokens in 2-dimensional space. Consequently, we apply a graph attention network [77] to the spatial adjacency graph to generate initial embedding for each cell token. This embedding is considered a conditional positional encoding (Cond PE) that encodes spatial neighborhoods while achieving translation invariance. Note that unlike CPVT [16], our graph-based Cond PE does not provide the absolute position. This is a desired outcome, as absolute positions are not as critical in spatial transcriptomics compared to images.

### 3.5 Discussions

We summarize all aforementioned positional encodings in Table 1. We consider four main properties when we compare these methods, namely relative position, global effectiveness, translation invariance, and structure awareness.

**Distance awareness** refers to the property that a positional encoding is able to indicate the pair-wise distance between two tokens, which is the most fundamental property that is needed by transformers for spatial transcriptomics, as mentioned in Section 1. The only encoding without this feature is RWPE. This is because RWPE aims for encoding local graph structure instead of relative positions.

**Global effectiveness** refers to the property that a positional encoding is able to indicate the relation between distant tokens. In other words, even if two tokens are very far apart, the positional encoding can still measure their distance. This is a double-edged

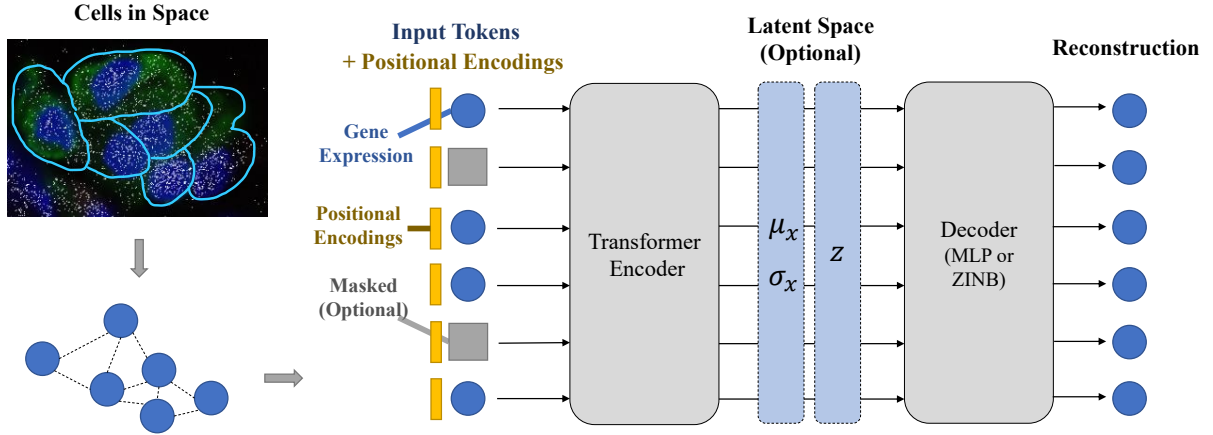


**Figure 1: An illustration of our transformer-based autoencoder framework for spatial transcriptomics data imputation.**

property. On the one hand, global PE enhances the ability of the transformer to capture long-range relevance between cells. On the other hand, it weakens the inductive bias of locality. This inductive bias, however, is effective for local cell-cell interactions. Cond PE imposes locality on the spatial adjacency graph, distinct from most other PEs.

**Translation invariance** refers to the property that a positional encoding stays invariant when the overall spatial coordinates are translated. Many previous studies [47, 68] have shown that this property is effective in enhancing the generalization ability of transformers. This property is also effective for spatial transcriptomics, and we therefore consider it an important feature in the selection of PE. Fortunately, graph-based position encodings typically possess this desirable property, as the translation of coordinates does not affect relative positions and therefore does not alter the spatial adjacency graph.

**Structure awareness** refers to the property that a positional encoding is able to encode the structure of space, such as density and homogeneity within local space, and the global spatial structure. This ability often comes from encoding the spatial graph, which goes beyond the definition of position encodings, but may provide additional information for transformers.

In conclusion, we investigate four types of position encoding to capture spatial information in transformers, which possess different properties and mostly demonstrate good potential as position encodings for spatial transcriptomics. We will apply distinct positional encodings in our SpaFormer framework in order to gain the best practices for position encoding in spatial transcriptomes.

## 4 OUR FRAMEWORK: SPAFORMER

In this section, we introduce our SpaFormer framework. An overview of SpaFormer is illustrated in Figure 1. In SpaFormer, we first extract the spatial positional encoding for each cell, using different methods as discussed in Section 3. Then cell embeddings are initialized with gene expressions and positional encodings, while some cells are selectively masked depending on the specific setting. Next, a transformer encoder is applied to encode both cellular profiles and intercellular contexts into the latent space. Finally, a decoder reconstructs the input (or masked) information based on the latent

variables. In the following, we first introduce our general framework that generalizes popular transcriptomic imputation models in Section 4.1. Then based on the general framework, we propose a new bi-level masking strategy in Section 4.2, which is particularly suitable for spatial transcriptomic data imputation.

### 4.1 Generalized Autoencoder Framework

The most popular architecture for deep-learning-based transcriptomic data imputation methods [4, 6, 29, 30, 59] is autoencoder, due to its prevalence in data denoising and missing data applications [29, 59, 79]. Existing methods introduced a few variants of autoencoders, including variational autoencoders (VAE) [37] and ZINB-based (zero-inflated negative binomial) autoencoders [25], while they often lack a systematic comparison for these autoencoder variants. In order to compare the performances of different autoencoders on the spatial transcriptomic imputation task, our SpaFormer framework generalizes both VAE and ZINB-based autoencoders, as well as vanilla autoencoders.

Our general framework takes a batch of cells as input. To be consistent with Section 2.1, we denote the input as  $\tilde{X} \in \mathcal{R}^{n \times k}$ , where  $n$  is the number of cells in the input field-of-view (FOV). Note that here we omit the positional encodings, which should also be included in the input matrix. An encoder  $q_\theta$  projects the input data to latent space, resulting in  $Z \in \mathcal{R}^{n \times d}$ , where  $d$  is the latent dimension. A decoder  $p_\phi$  then generates an output  $\hat{X} \in \mathcal{R}^{n \times k}$  from the latent space, where we expect  $\hat{X}$  to be identical with the input matrix  $\tilde{X}$ . The overall framework can be simply written as:

$$Z = q_\theta(\tilde{X}) \quad (13)$$

$$\hat{X} = p_\phi(Z) \quad (14)$$

Next, we proceed to introduce how we implement various autoencoder variants under the general framework.

**Vanilla autoencoders.** In the case of vanilla autoencoder, we implement  $q_\theta$  with a transformer and  $p_\phi$  with a multi-layer perception (MLP). Note that we have selected an asymmetrical encoder-decoder architecture, as we believe that the model requires a greater ability to utilize spatial information for denoising during the encoding

process. While during decoding, the contextual information of each cell has already been included in the latent space, making decoding easier. The loss function for vanilla autoencoders can be written as:

$$\mathcal{L}_{\text{MSE}} = \left\| \widehat{\mathbf{X}} - \widetilde{\mathbf{X}} \right\|_F^2 \quad (15)$$

**ZINB-based autoencoders.** Previous studies [25, 49, 64] pointed out that the data distribution of the transcriptomic data can be approximated by zero-inflated negative binomial (ZINB) distribution because the data are discrete, overdispersed and contain many zero values. Therefore, many recent methods [13, 27, 58, 62] in single-cell transcriptomic analysis adopt a ZINB-based autoencoder to leverage this prior information. A ZINB distribution is defined as:

$$\text{NB}(x | \mu, \theta) = \frac{\Gamma(x + \theta)}{x! \Gamma(\theta)} \left( \frac{\theta}{\theta + \mu} \right)^\theta \left( \frac{\mu}{\theta + \mu} \right)^x \quad (16)$$

$$\text{ZINB}(x | \pi, \mu, \theta) = \pi \delta_0(x) + (1 - \pi) \text{NB}(x) \quad (17)$$

where  $\mu$  and  $\pi$  denote mean and dispersion,  $\pi$  is the weight of the point mass at zero, and  $\delta_0$  generates constant 0.

In our SpaFormer framework, to adapt a vanilla autoencoder to a ZINB-based autoencoder, the encoder  $p_\phi$  remains unchanged, while a ZINB decoder implements the decoder  $q_\theta$  instead of an MLP decoder. A ZINB decoder takes the latent code  $Z$  as input and generates an intermediate result  $\widehat{H} \in \mathcal{R}^{n \times d'}$  via MLP. On top of that, ZINB decoders have three fully-connected output layers to estimate the parameters of ZINB distribution, denoted as:

$$\Pi = \text{sigmoid}(\widehat{H}W_\pi), M = \exp(\widehat{H}W_\mu), \Theta = \exp(\widehat{H}W_\theta) \quad (18)$$

where the output matrices  $\Pi$ ,  $M$  and  $\Theta$  correspond to the three parameters  $\pi, \mu, \theta$  of ZINB distribution in Eq. 17. ZINB decoder assumes that the input data are sampled from a ZINB distribution, therefore the overall loss function changes to the negative log-likelihood of the ZINB distribution, formulated as:

$$\mathcal{L}_{\text{ZINB}} = -\log(\text{ZINB}(\widetilde{\mathbf{X}} | \Pi, M, \Theta)) \quad (19)$$

In the inference stage, the estimated mean matrix  $M$  is selected as the imputation output.

**Variational autoencoders.** VAEs have been wildly applied in single-cell transcriptomic analysis [2, 9, 26, 38, 57, 74] since they are robust to technical noise and bias. They are also adopted for transcriptomic imputation in a few methods [48, 49]. In our SpaFormer framework, we optionally transform an autoencoder framework to a VAE by making modifications to the latent space and loss function. Specifically, two additional fully-connected layers are appended to the encoder to estimate the mean and variance of latent variables:

$$\mu_z = q_\theta(\widetilde{\mathbf{X}}) \cdot W_{\mu_z}, \quad \sigma_z = \exp(q_\theta(\widetilde{\mathbf{X}}) \cdot W_{\sigma_z}) \quad (20)$$

where  $\mu_z$  and  $\sigma_z$  are mean and variance respectively. The latent variables  $Z$  are then sampled from the estimated Gaussian distribution  $\mathcal{N}(\mu_z, \sigma_z)$ , where we apply reparametrization trick [37] to keep the gradient descend possible. Furthermore, an additional Kullback-Leibler (KL) divergence loss term is added to regularize the distribution of latent variables, which is:

$$\mathcal{L}_{\text{KL}} = D_{\text{KL}}(\mathcal{N}(\mu_z, \sigma_z) || \mathcal{N}(0, 1)) \quad (21)$$

For a vanilla autoencoder, the loss term turns to:

$$\mathcal{L} = \mathcal{L}_{\text{MSE}} + \beta \mathcal{L}_{\text{KL}} \quad (22)$$

where  $\beta$  is the KL loss weight. while for a ZINB-based autoencoder, the loss term turns to:

$$\mathcal{L} = \mathcal{L}_{\text{ZINB}} + \beta \mathcal{L}_{\text{KL}} \quad (23)$$

In the inference stage, we directly employ the estimated mean  $\mu_z$  as latent variables, instead of sampling.

## 4.2 Bi-level Masked Autoencoders

Inspired by the tremendous success of the masked autoencoding paradigm in NLP [19] and Computer Vision [32], we propose to incorporate a new masked autoencoder model into our generalized framework. Specifically, masked autoencoders are a form of more general denoising autoencoders [32, 79], which adopt a simple concept to remove a proportion of the data and then learn to recover the removed parts. The idea of masked autoencoders is also natural and applicable in spatial transcriptomics since we expect a powerful model to be able to recover missing cellular profiles from neighboring cells sharing the same microenvironment and homologous cells with the same cell state. Note that the objective of the masked autoencoder is highly consistent with the process of data imputation. Hence, it is very promising that the model will be trained with the specific capability for imputing missing values.

Despite that masked autoencoders are highly suitable for training an imputation model, the characteristic of spatial transcriptomics adds difficulties to the utilization of masked autoencoders. Compared to NLP and vision, it is much more difficult to recover cell profiles solely based on contexts. One reason is that the external signals a cell receives depend not only on the concentration of ligands in the microenvironment but also on the amount of receptors on its membrane. Therefore, it's hardly possible to identify intercellular correlations when the cell profile is completely masked out. To address this issue, we made a modification to the standard masked autoencoder, which we call it a bi-level masking strategy.

In a bi-level masking strategy, for each input batch of tokens, we first determine which cells are to be masked. Then, instead of thoroughly masking the tokens, we selectively mask out a certain proportion of features in those tokens, leaving the potential for the model to recover underlying intercellular correlations. Specifically, we first sample a mask vector  $\widetilde{\mathbf{m}}^{\text{token}} \in \{0, 1\}^n$  from a Bernoulli distribution with  $p = \theta$ , where  $n$  is the number of input tokens,  $\theta$  is the probability that a token is selected to be masked. Next,  $\widetilde{\mathbf{M}}^{\text{feat}} \in \{0, 1\}^{n \times k}$  is sampled from another Bernoulli distribution with  $p = \gamma$ , where  $\gamma$  is the probability that a feature is masked in a selected token. Lastly, we combined  $\widetilde{\mathbf{m}}^{\text{token}}$  and  $\widetilde{\mathbf{M}}^{\text{feat}}$  as:

$$\widetilde{\mathbf{M}}_{i,j} = 1 - \widetilde{\mathbf{m}}_i^{\text{token}} \cdot \widetilde{\mathbf{M}}_{i,j}^{\text{feat}} \quad (24)$$

where  $\widetilde{\mathbf{M}}$  is the finalized mask matrix. The input features  $\widetilde{\mathbf{X}}_{i,j}$  are then masked when  $\widetilde{\mathbf{M}}_{i,j} = 0$ , resulting in a new feature matrix  $\widetilde{\mathbf{X}}' \in \mathcal{R}^{n \times k}$  written as:

$$\widetilde{\mathbf{X}}' = \phi(\widetilde{\mathbf{M}} \odot \widetilde{\mathbf{X}}) \quad (25)$$

where  $\odot$  indicates element-wise multiplication, and  $\phi$  refers to a rescaling technique that maintains the mean of the input unchanged for each cell. Notably, when  $\gamma = 1$ , our masked autoencoder is equivalent to MAE for vision [32]. When  $\theta = 1$ , our masked autoencoder

is equivalent to a denoising autoencoder [79]. Such a bi-level masking strategy provides our framework with greater flexibility.

During training, masked features  $\tilde{X}'$  are used as initial token embeddings. Therefore, it should be plugged into Eq. 13 to replace  $\tilde{X}$ . Note that our bi-level masking strategy perfectly fits the overall autoencoder framework, which means we can combine the masked autoencoder with other components, i.e., VAE and ZINB decoders. When enabling the masked autoencoder, we need to change the reconstruction loss in Eq. 15 to:

$$\mathcal{L}_{\text{MSE}} = \left\| (1 - M') \odot (H - \tilde{X}) \right\|_F^2 \quad (26)$$

where we only calculate mean squared error (MSE) for the prediction of masked values. For inference, we simply dismiss the bi-level masking strategy. Instead, the unmasked input  $\tilde{X}$  is enabled, which provides extra information for imputation.

## 5 EXPERIMENT

### 5.1 Experimental settings

**5.1.1 Datasets.** We validate the proposed approach on three spatial transcriptomic datasets generated by the CosMX platform from Nanostring [33]. These datasets differ in their scales and sources of tissues, which highlights the comprehensiveness of our experiments. The data statistics are presented in Table 3.

**5.1.2 Baselines.** To evaluate the effectiveness of SpaFormer, we compare it with the state-of-the-art spatial and non-spatial transcriptomic imputation models: (1) scImpute [43] employs a probabilistic model to detect dropouts, and implements imputation through non-negative least squares regression. (2) SAVER [36] uses negative binomial distribution to model the data and estimates a Gamma prior through Poisson Lasso regression. The posterior mean is used to output expression with uncertainty quantification from the posterior distribution. (3) scVI [49] models dropouts with a ZINB distribution, and estimates the distributional parameters of each gene in each cell with a VAE model. (4) DCA [25] is an autoencoder that predicts parameters of chosen distributions like ZINB to generate the imputed data. (5) GraphSCI [62] employs a graph autoencoder on a gene correlation graph. Meanwhile, it uses another autoencoder to reconstruct the gene expressions, taking graph autoencoder embeddings as additional input. (6) scGNN [80] first builds a cell-cell graph based on gene expression similarity and then utilizes a graph autoencoder together with a standard autoencoder to refine graph structures and cell representation. Lastly, an imputation autoencoder is trained with a graph Laplacian smoothing term added to the reconstruction loss. (7) gimVI [48] is a deep generative model for integrating spatial transcriptomics data and scRNA-seq data which can be used to impute spatial transcriptomic data. gimVI is based on scVI [49] and employs alternative conditional distributions to address technology-specific covariate shift more effectively. (8) Sprod [42] is the latest published imputation method for spatial transcriptomics data. It first projects gene expressions to a latent space, then connects neighboring cells in the latent space, and prunes it with physical distance. Then a denoised matrix is learned by jointly minimizing the reconstruction error and a graph Laplacian smoothing term. (9) SpaGAT is a baseline model created by ourselves. It is the same bi-level masking autoencoder

framework as SpaFormer, based on a graph neural network encoder with spatial graphs. Specifically, we implement a graph attention network [77] as the encoder. Since the graph attention network is a localized version of transformers, SpaGAT can be considered an ablation study for our SpaFormer model.

Notably, we encountered scalability issues in scGNN and Sprod methods even with the smallest Kidney dataset. Both of these methods are designed based on cell-cell similarity graphs. scGNN trains neural networks on GPUs, however, it runs out of 300G CPU memory in an intermediate state when pruning the cell-cell graph. In contrast, Sprod separates data into numerous batches and purely runs on CPUs. We allocate 128 CPU processors for it, yet it fails to finish running in 48 hours.

**5.1.3 Implementation Settings.** Before we conduct the experiment, we first randomly mask 30% of the data to create the partially observed data, while the original masked data are considered as ground truth. All training and inference processes are then conducted on the partially observed data, and those dropped values are kept for evaluation. Based on the partially observed data, we further conduct preprocessing methods, according to the recommended settings of each specific model. For our own SpaGAT and SpaFormer, we first normalize the total RNA counts of each cell, and then apply log1p transform. In addition, considering that the output format of the baseline models varies between raw counts and log-transformed values, we uniformly conduct postprocessing to make sure all imputed data and ground-truth data are normalized and log-transformed. By default, SpaGAT and SpaFormer adopt a bi-level masked autoencoder, while SpaFormer chooses a Cond PE as positional encoding.

Regarding the evaluation, for imputation, the rooted mean squared error (RMSE), Pearson correlation coefficients (Pearson), and cosine similarity (Cosine) metrics are calculated based on the predictions of the masked values. For clustering, we first reduce the dimension of imputed data with PCA and then construct kNN graph based on the first 10 PCs. The clustering result is obtained from Leiden algorithm on the kNN graph, where we conduct a grid search to find the optimal resolution for Leiden. Clustering metrics normalized mutual information (NMI) and adjusted Rand index (ARI) are then calculated based on the clustering results and predefined cell type labels. Lastly, all deep learning models are evaluated with 5 random seeds, and the average performance is reported, while statistical models are evaluated only once.

### 5.2 Imputation Performance

In Table 2, we present the experimental results. It is shown that our SpaFormer consistently outperforms other baselines by showing a better imputation performance. Aside from that, there are several interesting observations. (1) scVI and DCA consistently present suboptimal performance, outperforming some advanced methods, e.g., GraphSCI. In fact, this result is consistent with a recent transcriptomic imputation benchmark [17]. Since both DCA and scVI adopt ZINB-based autoencoders, this demonstrates the effectiveness of ZINB-based autoencoders. (2) gimVI does not work well on our highly noisy spatial transcriptomic dataset. gimVI is a famous reference-based model that maps spatial transcriptomic data to

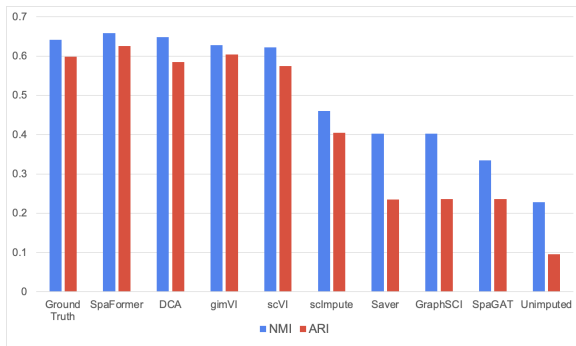
**Table 2: Imputation performance on three CosMx datasets.**

	Lung 5				Kidney 1139				Liver Normal		
	RMSE↓	Pearson↑	Cosine↑	RMSE↓	Pearson↑	Cosine↑	RMSE↓	Pearson↑	Cosine↑		
Unimputed	0.3758	-	-	0.3747	-	-	0.3507	-	-		
scImpute	0.3245	0.444	0.5214	0.311	0.4824	0.5714	0.3048	0.4437	0.5074		
SAVER	0.3213	0.4564	0.5269	0.3106	0.4887	0.5689	0.2909	0.5462	0.5864		
scVI	0.2861	<u>0.6231</u>	<u>0.6661</u>	0.2901	0.5834	0.648	0.2797	0.5749	0.6224		
DCA	<u>0.2858</u>	0.6223	0.6648	<u>0.2852</u>	<u>0.5985</u>	<u>0.6597</u>	0.2542	0.657	0.688		
GraphSCI	0.3957	0.1334	0.3081	0.3624	0.2403	0.4128	0.3347	0.3707	0.443		
gimVI	0.317	0.532	0.5917	0.4387	-0.0104	0.1967	0.4542	-0.0015	0.117		
scGNN		OOM <sup>1</sup>			OOM <sup>1</sup>			OOM <sup>1</sup>			
Sprod		OOT <sup>2</sup>			OOT <sup>2</sup>			OOT <sup>2</sup>			
SpaGAT	0.2865	0.6047	0.6518	0.2859	0.5852	0.6506	<u>0.2241</u>	<u>0.7624</u>	<u>0.7829</u>		
SpaFormer	<b>0.2785</b>	<b>0.6363</b>	<b>0.6786</b>	<b>0.2794</b>	<b>0.6108</b>	<b>0.671</b>	<b>0.2117</b>	<b>0.7793</b>	<b>0.7973</b>		

<sup>1</sup> Run out of 300G CPU Memory.<sup>2</sup> Run more than 48 hours on 128 CPUs.**Table 3: Dataset statistics.**

Dataset	Cell Num.	FOV Num.	Gene Num.	Zero Ratio
Lung 5	99,656	30	960	86.74%
Kidney 1139	61,283	18	960	83.49%
Liver Normal	305,730	244	1000	86.39%

scRNA-seq reference datasets. In our experiments, we prepare several reference datasets for gimVI. However, since our dataset only covers less than 1000 genes and the data is very sparse, gimVI's mapping accuracy is quite low. This shows a potential problem with the reference-based imputation approaches. (3) SpaGAT, the non-transformer version of SpaFormer, presents fairly good performance, which demonstrates the advantage of our bi-level mask-autoencoder framework.

**Figure 2: Clustering performance on Lung dataset.**

### 5.3 Clustering Performance

In addition to imputation performance, we evaluate clustering performance as well. For evaluation, cell type labels accompanied by the dataset are considered as ground truth. It is expected that well-imputed data can better recover the cell clustering structures. As shown in Figure 2, although all models enhance the clustering performance as compared to the unimputed data, clustering based on SpaFormer achieves better performance. It is worth noting that

despite SpaGAT achieving competitive performance for imputation, the clustering performance of SpaGAT is considerably bad. This is because SpaGAT only leverages the information of spatially adjacent cells, without considering homology among global cells.

To clarify, we only present the clustering performance on the Lung dataset, since our domain expert noticed that the cell type labels of the other two datasets do not show a strong correlation with real cell clusters. As a result, all models perform evenly poor on the other two datasets.

### 5.4 Ablation Study

**5.4.1 Positional Encodings.** As we mentioned in Section 3, we conduct experiments on three datasets to compare the performance of different positional encodings. According to our experiments in Figure 3, Cond PE and LapPE outperform other positional encodings w.r.t overall performance on three datasets, indicating the effectiveness of graph-based PEs. Meanwhile, Cond PE outperforms SignNet, suggesting that global effectiveness might not be a desired property for spatial transcriptomics, as we discussed in Section 3.5. In conclusion, we select Cond PE as a default setting in SpaFormer. Besides, a 2-dimensional Sinusoid PE can also be a good choice for spatial transcriptomics since it has fewer parameters than others. Meanwhile, the gap between transformers with and without positional encodings is less significant than we expected. Therefore, there is still large room for exploration in positional encodings for spatial transcriptomic data.

**5.4.2 Autoencoder Frameworks.** Another highlight of our SpaFormer framework is that we generalize different popular autoencoder-based models. Based on our general framework, we conduct a thorough ablation study on the Liver dataset. The experimental results in Figure 4 indicate that various variations of autoencoders achieved optimal performance when combined with masking. Additionally, the simple bi-level mask autoencoder obtained the best results. Therefore, we recommend the masked autoencoder as the default setting for our SpaFormer framework.

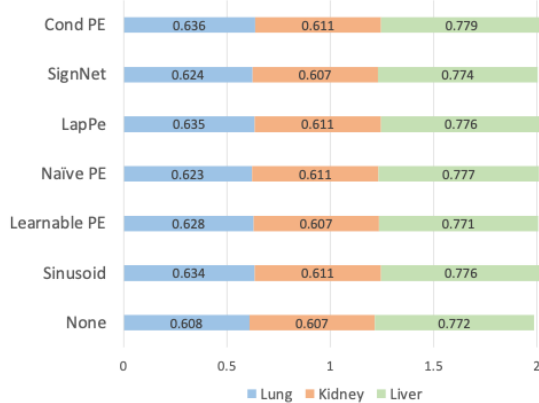


**Figure 3: Comparison between different positional encodings on three datasets. Values indicate Pearson correlation coefficient.**

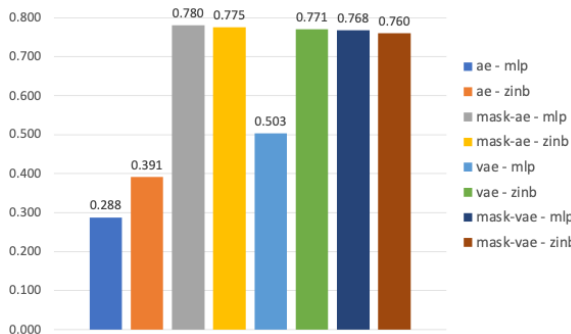


**Figure 4: Ablation study on different autoencoder variants, i.e., autoencoders (ae) and variational autoencoders (vae), w. and w/o masking, mlp and zinb decoders. Values indicate Pearson correlation coefficient on Liver dataset.**

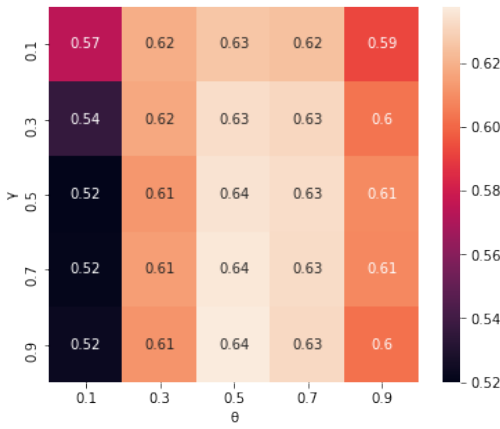


**Figure 5: Ablation study on parameter  $\theta$  and  $\gamma$ . Values indicate Pearson correlation coefficient on Lung dataset.**

**5.4.3 Mask Ratio.** Lastly, we conduct an ablation study on token masked ratio  $\theta$  and feature masked ratio  $\gamma$  in Section 4.2 to demonstrate the importance of our bi-level masking strategy. As shown in Figure 5, joint tuning  $\theta$  and  $\gamma$  results in an optimal Pearson correlation score. In our main experiment, we select  $\theta = 0.5$ ,  $\gamma = 0.5$  as

default parameters, since this setting consistently achieves optimal performance on three datasets.

## 6 RELATED WORK

### 6.1 Spatially Resolved Transcriptomics

Recently, spatial transcriptomic technologies are developed to spatially resolve transcriptomics profiles [56, 70]. With spatial transcriptomics data, researchers can learn the spatial context of cells and cell clusters within a tissue [8]. The major technologies/platforms for spatial transcriptomics are Visium by 10x [70], GeoMx Digital Spatial Profiler (DSP) [56] by NanoString and CosMx Spatial Molecular Imager (SMI) by NanoString, MERFISH, Vizgen, Resolve, Rebus, and molecular cartography. 10x Visium does not profile at single-cell resolution, and while GeoMx DSP is capable of single-cell resolution through user-drawn profiling regions, the scalability is limited. The most recent platform, CosMx Spatial Molecular Imager (SMI) [33], can profile consistently at single-cell and even subcellular resolution. CosMx SMI follows much of the initial protocol as GeoMx DSP, with barcoding and ISH hybridization. However, the SMI instrument performs 16 cycles of automated cyclic readout, and in each cycle, the set of barcodes (readouts) are UV-cleaved and removed. These cycles of hybridization and imaging yield spatially resolved profiling of RNA and protein at single-cell ( $\sim 10\mu\text{m}$ ) and subcellular ( $\sim 1\mu\text{m}$ ) resolution. In this work, we use two published and one unpublished dataset produced by the CosMx platform. In order to obtain the cellular level gene expression, CellPose [69] software is applied to conduct cell segmentation.

### 6.2 Single-cell Transcriptomics Data Imputation

The increased resolution of transcriptomics profiling methods comes at a cost of increasing data sparsity. The profiling technology may fail to capture a number of the expressed genes of an individual cell due to low amounts of mRNA in individual cells and a low capture rate. A popular way to address this issue is to perform imputation, which aims to correct false zeros by estimating realistic values for those gene-cell pairs. A large number of methods have been developed for the task of scRNA-seq data imputation, mainly focusing on generative probability models or matrix factorization [31, 36, 66, 75]. Aside from these methods, deep learning models have gained immense popularity over recent years. A natural deep learning architecture for the imputation task is the autoencoder, due to its prevalence in data denoising and missing data applications [4, 6, 29, 30, 59].

To leverage the spatial information of spatial transcriptomic data, the latest method, Sprod [82] constructs a graph by connecting cells with similar transcriptomic profiles and prunes it with physical distance. Then a denoised matrix is learned by minimizing the reconstruction error and a graph Laplacian smoothing term. However, this graph only connects cells that are spatially close to each other. As a result, it is limited in a localized spatial context and difficult to identify cells with long-range correlations. Different from the aforementioned methods, we propose to utilize transformers for spatial transcriptomic imputation to globally model the cell-cell interactions while exploiting the spatial information.

## 7 CONCLUSION

In this work, we comprehensively investigate two key questions related to implementing transformer models for spatial transcriptomic imputation at the cellular level. By answering these two questions, we proposed a transformer-based general imputation framework *SpaFormer* for spatial transcriptomics data. In addition, we propose a new bi-level masking technique, which can be incorporated into general autoencoder frameworks. Our method outperforms all existing methods for recovering missing values and clustering structures.

## REFERENCES

- [1] Hassan Akbari, Liangzhe Yuan, Rui Qian, Wei-Hong Chuang, Shih-Fu Chang, Yin Cui, and Boqing Gong. 2021. Vatt: Transformers for multimodal self-supervised learning from raw video, audio and text. *Advances in Neural Information Processing Systems* 34 (2021), 24206–24221.
- [2] Ricard Argelaguet, Damien Arnol, Daniela Bredikhin, Yonatan Deloro, Britta Velten, John C Marioni, and Oliver Stegle. 2020. MOFA+: a statistical framework for comprehensive integration of multi-modal single-cell data. *Genome biology* 21, 1 (2020), 1–17.
- [3] Chiara Baccin, Jude Al-Sabah, Lars Velten, Patrick M Helbling, Florian Grünschläger, Pablo Hernández-Malmierca, César Nombela-Arrieta, Lars M Steinmetz, Andreas Trumpp, and Simon Haas. 2020. Combined single-cell and spatial transcriptomics reveal the molecular, cellular and spatial bone marrow niche organization. *Nature cell biology* 22, 1 (2020), 38–48.
- [4] Brett K Beaulieu-Jones, Jason H Moore, and POOLED RESOURCE OPEN-ACCESS ALS CLINICAL TRIALS CONSORTIUM. 2017. Missing data imputation in the electronic health record using deeply learned autoencoders. In *Pacific symposium on biocomputing* 2017. World Scientific, 207–218.
- [5] Mikhail Belkin and Partha Niyogi. 2003. Laplacian eigenmaps for dimensionality reduction and data representation. *Neural computation* 15, 6 (2003), 1373–1396.
- [6] Guillen Boquet, Jose Lopez Vicario, Antoni Morell, and Javier Serrano. 2019. Missing data in traffic estimation: A variational autoencoder imputation method. In *ICASSP 2019-2019 IEEE International Conference on Acoustics, Speech and Signal Processing (ICASSP)*. IEEE, 2882–2886.
- [7] Robin Browaeys, Wouter Saelens, and Yvan Saeys. 2020. NicheNet: modeling intercellular communication by linking ligands to target genes. *Nature methods* 17, 2 (2020), 159–162.
- [8] Darren J Burgess. 2019. Spatial transcriptomics coming of age. *Nature Reviews Genetics* 20, 6 (2019), 317–317.
- [9] Zhi-Jie Cao and Ge Gao. 2022. Multi-omics single-cell data integration and regulatory inference with graph-linked embedding. *Nature Biotechnology* 40, 10 (2022), 1458–1466.
- [10] Nicolas Carion, Francisco Massa, Gabriel Synnaeve, Nicolas Usunier, Alexander Kirillov, and Sergey Zagoruyko. 2020. End-to-end object detection with transformers. In *Computer Vision–ECCV 2020: 16th European Conference, Glasgow, UK, August 23–28, 2020, Proceedings, Part I* 16. Springer, 213–229.
- [11] Dexiong Chen, Leslie O’Bray, and Karsten Borgwardt. 2022. Structure-aware transformer for graph representation learning. In *International Conference on Machine Learning*. PMLR, 3469–3489.
- [12] Kok Hao Chen, Alistair N Boettiger, Jeffrey R Moffitt, Siyuan Wang, and Xiaowei Zhuang. 2015. Spatially resolved, highly multiplexed RNA profiling in single cells. *Science* 348, 6233 (2015), aaa6090.
- [13] Liang Chen, Weinan Wang, Yuyao Zhai, and Minghua Deng. 2020. Deep soft K-means clustering with self-training for single-cell RNA sequence data. *NAR genomics and bioinformatics* 2, 2 (2020), lqa039.
- [14] Krzysztof Choromanski, Valerii Likhoshesterov, David Dohan, Xingyou Song, Andreea Gane, Tamas Sarlos, Peter Hawkins, Jared Davis, Afroz Mohiuddin, Lukasz Kaiser, et al. 2020. Rethinking attention with performers. *arXiv preprint arXiv:2009.14794* (2020).
- [15] Krzysztof Marcin Choromanski, Valerii Likhoshesterov, David Dohan, Xingyou Song, Andreea Gane, Tamas Sarlos, Peter Hawkins, Jared Quincy Davis, Afroz Mohiuddin, Lukasz Kaiser, David Benjamin Belanger, Lucy J Colwell, and Adrian Weller. 2021. Rethinking Attention with Performers. In *International Conference on Learning Representations*.
- [16] Xiangxiang Chu, Zhi Tian, Bo Zhang, Xinlong Wang, Xiaolin Wei, Huaxia Xia, and Chunhua Shen. 2021. Conditional positional encodings for vision transformers. *arXiv preprint arXiv:2102.10882* (2021).
- [17] Chichi Dai, Yi Jiang, Chenglin Yin, Ran Su, Xiangxiang Zeng, Quan Zou, Kenta Nakai, and Leyi Wei. 2022. scIMC: a platform for benchmarking comparison and visualization analysis of scRNA-seq data imputation methods. *Nucleic Acids Research* 50, 9 (2022), 4877–4899.
- [18] Yue Deng, Feng Bao, Qionghai Dai, Lani F Wu, and Steven J Altschuler. 2018. Massive single-cell RNA-seq analysis and imputation via deep learning. *BioRxiv* (2018), 315556.
- [19] Jacob Devlin, Ming-Wei Chang, Kenton Lee, and Kristina Toutanova. 2018. Bert: Pre-training of deep bidirectional transformers for language understanding. *arXiv preprint arXiv:1810.04805* (2018).
- [20] David van Dijk, Juozas Nainys, Roshan Sharma, Pooja Kaithal, Ambrose J Carr, Kevin R Moon, Linas Mazutis, Guy Wolf, Smita Krishnaswamy, and Dana Pe’er. 2017. MAGIC: A diffusion-based imputation method reveals gene-gene interactions in single-cell RNA-sequencing data. *BioRxiv* (2017), 111591.
- [21] Kangning Dong and Shihua Zhang. 2022. Deciphering spatial domains from spatially resolved transcriptomics with an adaptive graph attention auto-encoder. *Nature communications* 13, 1 (2022), 1–12.
- [22] Alexey Dosovitskiy, Lucas Beyer, Alexander Kolesnikov, Dirk Weissenborn, Xiaohua Zhai, Thomas Unterthiner, Mostafa Dehghani, Matthias Minderer, Georg Heigold, Sylvain Gelly, et al. 2020. An image is worth 16x16 words: Transformers

for image recognition at scale. *arXiv preprint arXiv:2010.11929* (2020).

[23] Vijay Prakash Dwivedi, Anh Tuan Luu, Thomas Laurent, Yoshua Bengio, and Xavier Bresson. 2021. Graph neural networks with learnable structural and positional representations. *arXiv preprint arXiv:2110.07875* (2021).

[24] Chee-Huat Linus Eng, Michael Lawson, Qian Zhu, Ruben Dries, Noushin Koulen, Yodai Takei, Jim Yun, Christopher Cronin, Christoph Karp, Guo-Cheng Yuan, et al. 2019. Transcriptome-scale super-resolved imaging in tissues by RNA seqFISH+. *Nature* 568, 7751 (2019), 235–239.

[25] Gökçen Eraslan, Lukas M Simon, Maria Mircea, Nikola S Mueller, and Fabian J Theis. 2019. Single-cell RNA-seq denoising using a deep count autoencoder. *Nature communications* 10, 1 (2019), 390.

[26] Huazhu Fu, Hang Xu, Kelvin Chong, Mengwei Li, Kok Siong Ang, Hong Kai Lee, Jingjing Ling, Ao Chen, Ling Shao, Longqi Liu, et al. 2021. Unsupervised spatially embedded deep representation of spatial transcriptomics. *Biorxiv* (2021), 2021–06.

[27] Yanglan Gan, Xingyu Huang, Guobing Zou, Shuigeng Zhou, and Jihong Guan. 2022. Deep structural clustering for single-cell RNA-seq data jointly through autoencoder and graph neural network. *Briefings in Bioinformatics* 23, 2 (2022).

[28] Amin Ghiasi, Hamid Kazemi, Eitan Borgnia, Steven Reich, Manli Shu, Micah Goldblum, Andrew Gordon Wilson, and Tom Goldstein. 2022. What do Vision Transformers Learn? A Visual Exploration. *arXiv preprint arXiv:2212.06727* (2022).

[29] Lovedeep Gondara and Ke Wang. 2017. Multiple imputation using deep denoising autoencoders. *arXiv preprint arXiv:1705.02737* 280 (2017).

[30] Lovedeep Gondara and Ke Wang. 2018. Mida: Multiple imputation using denoising autoencoders. In *Pacific-Asia conference on knowledge discovery and data mining*. Springer, 260–272.

[31] Wuming Gong, Il-Youp Kwak, Pruthvi Pota, Naoko Koyano-Nakagawa, and Daniel J Garry. 2018. DrImpute: imputing dropout events in single cell RNA sequencing data. *BMC bioinformatics* 19, 1 (2018), 1–10.

[32] Kaiming He, Xinlei Chen, Saining Xie, Yanghao Li, Piotr Dollár, and Ross Girshick. 2022. Masked autoencoders are scalable vision learners. In *Proceedings of the IEEE/CVF Conference on Computer Vision and Pattern Recognition*. 16000–16009.

[33] Shanshan He, Ruchir Bhatt, Carl Brown, Emily A. Brown, Derek L. Buhr, Kan Chantranuwatana, Patrick Danaher, Dwayne Dunaway, Ryan G. Garrison, Gary Geiss, Mark T. Gregory, Margaret L. Hoang, Rustem Khaifizov, Emily E. Killingbeck, Dae Kim, Tae Kyung Kim, Youngmi Kim, Andrew Klock, Mithra Korukonda, Aleksandr Kutchma, Zachary R. Lewis, Yan Liang, Jeffrey S. Nelson, Giang T. Ong, Evan P. Perillo, Joseph C. Phan, Tien Phan-Everson, Erin Piazza, Tushar Rane, Zachary Reitz, Michael Rhodes, Alyssa Rosenblum, David Ross, Hiromi Sato, Aster W. Wardhani, Corey A. Williams-Wietzikoski, Lidan Wu, and Joseph M. Beechem. 2022. High-plex Multiomic Analysis in FFPE at Subcellular Level by Spatial Molecular Imaging. *bioRxiv* (2022). <https://doi.org/10.1101/2021.11.03.467020>

[34] Jian Hu, Xiangjie Li, Kyle Coleman, Amelia Schroeder, Nan Ma, David J Irwin, Edward B Lee, Russell T Shinohara, and Mingyao Li. 2021. SpaGCN: Integrating gene expression, spatial location and histology to identify spatial domains and spatially variable genes by graph convolutional network. *Nature methods* 18, 11 (2021), 1342–1351.

[35] Kenneth H Hu, John P Eichorst, Chris S McGinnis, David M Patterson, Eric D Chow, Kelly Kersten, Stephen C Jameson, Zev J Gartner, Arjun A Rao, and Matthew F Krummel. 2020. ZipSeq: barcoding for real-time mapping of single cell transcriptomes. *Nature methods* 17, 8 (2020), 833–843.

[36] Mo Huang, Jingshu Wang, Eduardo Torre, Hannah Dueck, Sydney Shaffer, Roberto Bonasio, John I Murray, Arjun Raj, Mingyao Li, and Nancy R Zhang. 2018. SAVER: gene expression recovery for single-cell RNA sequencing. *Nature methods* 15, 7 (2018), 539–542.

[37] Diederik P Kingma and Max Welling. 2013. Auto-encoding variational bayes. *arXiv preprint arXiv:1312.6114* (2013).

[38] Vitalii Kleshchevnikov, Artem Shmatko, Emma Dann, Alexander Aivazidis, Hamish W King, Tong Li, Rasa Elmentaita, Artem Lomakin, Veronika Kedian, Adam Gayoso, et al. 2022. Cell2location maps fine-grained cell types in spatial transcriptomics. *Nature biotechnology* 40, 5 (2022), 661–671.

[39] Devin Kreuzer, Dominique Beaini, Will Hamilton, Vincent Létourneau, and Prudencio Tossou. 2021. Rethinking graph transformers with spectral attention. *Advances in Neural Information Processing Systems* 34 (2021), 21618–21629.

[40] Je Hyul Lee, Evan R Daugherty, Jonathan Scheiman, Reza Kalhor, Thomas C Ferrante, Richard Terry, Brian M Turczyk, Joyce L Yang, Ho Suk Lee, John Aach, et al. 2015. Fluorescent in situ sequencing (FISSEQ) of RNA for gene expression profiling in intact cells and tissues. *Nature protocols* 10, 3 (2015), 442–458.

[41] Dongshunyi Li, Jun Ding, and Ziv Bar-Joseph. 2021. Identifying signaling genes in spatial single-cell expression data. *Bioinformatics* 37, 7 (2021), 968–975.

[42] Jiachen Li, Siheng Chen, Xiaoyong Pan, Ye Yuan, and Hong-Bin Shen. 2022. Cell clustering for spatial transcriptomics data with graph neural networks. *Nature Computational Science* 2, 6 (2022), 399–408.

[43] Wei Vivian Li and Jingyi Jessica Li. 2018. An accurate and robust imputation method scImpute for single-cell RNA-seq data. *Nature communications* 9, 1 (2018), 1–9.

[44] Zhuli Li, Tianci Song, Jeongsik Yong, and Rui Kuang. 2021. Imputation of spatially-resolved transcriptomes by graph-regularized tensor completion. *PLoS computational biology* 17, 4 (2021), e1008218.

[45] Derek Lim, Joshua Robinson, Lingxiao Zhao, Tess Smidt, Suvrit Sra, Haggai Maron, and Stefanie Jegelka. 2022. Sign and basis invariant networks for spectral graph representation learning. *arXiv preprint arXiv:2202.13013* (2022).

[46] Tianyang Lin, Yuxin Wang, Xiangyang Liu, and Xipeng Qiu. 2022. A survey of transformers. *AI Open* (2022).

[47] Ze Liu, Yutong Lin, Yue Cao, Han Hu, Yixuan Wei, Zheng Zhang, Stephen Lin, and Baining Guo. 2021. Swin transformer: Hierarchical vision transformer using shifted windows. In *Proceedings of the IEEE/CVF international conference on computer vision*. 10012–10022.

[48] Romain Lopez, Achille Nazaret, Maxime Langevin, Jules Samaran, Jeffrey Regier, Michael I Jordan, and Nir Yosef. 2019. A joint model of unpaired data from scRNA-seq and spatial transcriptomics for imputing missing gene expression measurements. *arXiv preprint arXiv:1905.02269* (2019).

[49] Romain Lopez, Jeffrey Regier, Michael B Cole, Michael I Jordan, and Nir Yosef. 2018. Deep generative modeling for single-cell transcriptomics. *Nature methods* 15, 12 (2018), 1053–1058.

[50] Ery Lubeck, Ahmet F Coskun, Timur Zhiyentayev, Mubhij Ahmad, and Long Cai. 2014. Single-cell in situ RNA profiling by sequential hybridization. *Nature methods* 11, 4 (2014), 360–361.

[51] Shengjie Luo, Shanda Li, Tianle Cai, Di He, Dinglan Peng, Shuxin Zheng, Guolin Ke, Liwei Wang, and Tie-Yan Liu. 2021. Stable, fast and accurate: Kernelized attention with relative positional encoding. *Advances in Neural Information Processing Systems* 34 (2021), 22795–22807.

[52] Ying Ma and Xiang Zhou. 2022. Spatially informed cell-type deconvolution for spatial transcriptomics. *Nature Biotechnology* (2022), 1–11.

[53] Silas Maniatis, Joana Petrescu, and Hemali Phatnani. 2021. Spatially resolved transcriptomics and its applications in cancer. *Current opinion in genetics & development* 66 (2021), 70–77.

[54] Kristen R Maynard, Leonardo Collado-Torres, Lukas M Weber, Cedric Uytengco, Brianna K Barry, Stephen R Williams, Joseph L Catallini, Matthew N Tran, Zachary Besich, Madhavi Tippani, et al. 2021. Transcriptome-scale spatial gene expression in the human dorsolateral prefrontal cortex. *Nature neuroscience* 24, 3 (2021), 425–436.

[55] Chiara Medaglia, Amir Giladi, Liat Stoler-Barak, Marco De Giovanni, Tomer Meir Salame, Adi Biram, Eyal David, Hanjie Li, Matteo Iannaccone, Ziv Shulman, et al. 2017. Spatial reconstruction of immune niches by combining photoactivatable reporters and scRNA-seq. *Science* 358, 6370 (2017), 1622–1626.

[56] Christopher R Merritt, Giang T Ong, Sarah E Church, Kristi Barker, Patrick Danaher, Gary Geiss, Margaret Hoang, Jaemyeong Jung, Yan Liang, Jill McKay-Fleisch, et al. 2020. Multiplex digital spatial profiling of proteins and RNA in fixed tissue. *Nature Biotechnology* (05 2020). <https://doi.org/10.1038/s41587-020-0472-9>

[57] Kodai Minoura, Ko Abe, Hyunha Nam, Hiroyoshi Nishikawa, and Teppei Shimamura. 2021. scMM: Mixture-of-experts multimodal deep generative model for single-cell multiomics data analysis. *bioRxiv* (2021), 2021–02.

[58] Dylan Molho, Jiayuan Ding, Zhaoheng Li, Hongzhi Wen, Wenzhuo Tang, Yixin Wang, Julian Venegas, Wei Jin, Renming Liu, Runze Su, et al. 2022. Deep Learning in Single-Cell Analysis. *arXiv preprint arXiv:2210.12385* (2022).

[59] Ricardo Cardoso Pereira, Miriam Seoane Santos, Pedro Pereira Rodrigues, and Pedro Henriquez Abreu. 2020. Reviewing autoencoders for missing data imputation: Technical trends, applications and outcomes. *Journal of Artificial Intelligence Research* 69 (2020), 1255–1285.

[60] Zhen Qin, Weixuan Sun, Hui Deng, Dongxu Li, Yunshen Wei, Baohong Lv, Junjie Yan, Lingpeng Kong, and Yiran Zhong. 2022. coformer: Rethinking softmax in attention. *arXiv preprint arXiv:2202.08791* (2022).

[61] Ladislav Rampášek, Mikhail Galkin, Vijay Prakash Dwivedi, Anh Tuan Luu, Guy Wolf, and Dominique Beaini. 2022. Recipe for a general, powerful, scalable graph transformer. *arXiv preprint arXiv:2205.12454* (2022).

[62] Jiahua Rao, Xiang Zhou, Yutong Lu, Huiyong Zhao, and Yuedong Yang. 2021. Imputing single-cell RNA-seq data by combining graph convolution and autoencoder neural networks. *Iscience* 24, 5 (2021), 102393.

[63] Emily Reif, Ann Yuan, Martin Wattenberg, Fernanda B Viegas, Andy Coenen, Adam Pearce, and Been Kim. 2019. Visualizing and measuring the geometry of BERT. *Advances in Neural Information Processing Systems* 32 (2019).

[64] Davide Risso, Fanny Perraudeau, Svetlana Gribkova, Sandrine Dudoit, and Jean-Philippe Vert. 2018. A general and flexible method for signal extraction from single-cell RNA-seq data. *Nature communications* 9, 1 (2018), 284.

[65] Samuel G Rodrigues, Robert R Stickels, Aleksandrina Goeva, Carly A Martin, Evan Murray, Charles R Vanderburg, Joshua Welch, Linlin M Chen, Fei Chen, and Evan Z Macosko. 2019. Slide-seq: A scalable technology for measuring genome-wide expression at high spatial resolution. *Science* 363, 6434 (2019), 1463–1467.

[66] Jonathan Ronen and Altuna Akalin. 2018. netSmooth: Network-smoothing based imputation for single cell RNA-seq. *F1000Research* 7 (2018).

[67] Alexander Y Rudensky. 2011. Regulatory T cells and Foxp3. *Immunological reviews* 241, 1 (2011), 260–268.

- [68] Peter Shaw, Jakob Uszkoreit, and Ashish Vaswani. 2018. Self-Attention with Relative Position Representations. In *Proceedings of the 2018 Conference of the North American Chapter of the Association for Computational Linguistics: Human Language Technologies, Volume 2 (Short Papers)*. 464–468.
- [69] Carseen Stringer, Tim Wang, Michalis Michaelos, and Marius Pachitariu. 2021. Cellpose: a generalist algorithm for cellular segmentation. *Nature methods* 18, 1 (2021), 100–106.
- [70] Patrik L. Ståhl, Fredrik Salmén, Sanja Vickovic, Anna Lundmark, José Fernández Navarro, Jens Magnusson, Stefania Giacomello, Michaela Asp, Jakub O. Westholm, Mikael Huss, Annelie Mollbrink, Sten Linnarsson, Simone Codeluppi, Åke Borg, Fredrik Pontén, Paul Igor Costea, Pelin Sahlén, Jan Mulder, Olaf Bergmann, Joakim Lundeberg, and Jonas Frisén. 2016. Visualization and analysis of gene expression in tissue sections by spatial transcriptomics. *Science* 353, 6294 (2016), 78–82. <https://doi.org/10.1126/science.aaf2403>
- [71] Divyanshu Talwar, Aanchal Mongia, Debarka Sengupta, and Angshul Majumdar. 2018. AutoImpute: Autoencoder based imputation of single-cell RNA-seq data. *Scientific reports* 8, 1 (2018), 1–11.
- [72] Wenhao Tang, François Bertaux, Philipp Thomas, Claire Stefanelli, Malika Saint, Samuel Marguerat, and Vahid Shahrezaei. 2020. bayNorm: Bayesian gene expression recovery, imputation and normalization for single-cell RNA-sequencing data. *Bioinformatics* 36, 4 (2020), 1174–1181.
- [73] Hugo Touvron, Matthieu Cord, Matthijs Douze, Francisco Massa, Alexandre Sablayrolles, and Hervé Jégou. 2021. Training data-efficient image transformers & distillation through attention. In *International conference on machine learning*. PMLR, 10347–10357.
- [74] Duc Tran, Hung Nguyen, Bang Tran, Carlo La Vecchia, Hung N Luu, and Tin Nguyen. 2021. Fast and precise single-cell data analysis using a hierarchical autoencoder. *Nature communications* 12, 1 (2021), 1029.
- [75] David van Dijk, Juozas Nainys, Roshan Sharma, Pooja Kaithail, Ambrose J Carr, Kevin R Moon, Linas Mazutis, Guy Wolf, Smita Krishnaswamy, and Dana Pe'er. 2017. MAGIC: A diffusion-based imputation method reveals gene–gene interactions in single-cell RNA-sequencing data. *BioRxiv* (2017), 111591.
- [76] Ashish Vaswani, Noam Shazeer, Niki Parmar, Jakob Uszkoreit, Llion Jones, Aidan N Gomez, Łukasz Kaiser, and Illia Polosukhin. 2017. Attention is all you need. *Advances in neural information processing systems* 30 (2017).
- [77] Petar Veličković, Guillem Cucurull, Arantxa Casanova, Adriana Romero, Pietro Lio, and Yoshua Bengio. 2017. Graph attention networks. *arXiv preprint arXiv:1710.10903* (2017).
- [78] Sanja Vickovic, Gökçen Eraslan, Fredrik Salmén, Johanna Klughammer, Linnea Stenbeck, Deniz Schapiro, Tarmo Áijö, Richard Bonneau, Ludvig Bergenstråhl, José Fernández Navarro, et al. 2019. High-definition spatial transcriptomics for in situ tissue profiling. *Nature methods* 16, 10 (2019), 987–990.
- [79] Pascal Vincent, Hugo Larochelle, Yoshua Bengio, and Pierre-Antoine Manzagol. 2008. Extracting and composing robust features with denoising autoencoders. In *Proceedings of the 25th international conference on Machine learning*. 1096–1103.
- [80] Juexin Wang, Anjun Ma, Yuzhou Chang, Jianting Gong, Yue Xu, Ren Qi, Cankun Wang, Hongjun Fu, Qin Ma, and Dong Xu. 2021. scGNN is a novel graph neural network framework for single-cell RNA-Seq analyses. *Nature communications* 12, 1 (2021), 1–11.
- [81] Sinong Wang, Belinda Z Li, Madian Khabsa, Han Fang, and Hao Ma. 2020. Linformer: Self-attention with linear complexity. *arXiv preprint arXiv:2006.04768* (2020).
- [82] Yunguan Wang, Bing Song, Shidan Wang, Mingyi Chen, Yang Xie, Guanghua Xiao, Li Wang, and Tao Wang. 2022. Sprod for de-noising spatially resolved transcriptomics data based on position and image information. *Nature methods* 19, 8 (2022), 950–958.
- [83] Zelun Wang and Jyh-Charn Liu. 2021. Translating math formula images to LaTeX sequences using deep neural networks with sequence-level training. *International Journal on Document Analysis and Recognition (IJDAR)* 24, 1-2 (2021), 63–75.
- [84] Hongzhi Wen, Wei Jin, Jiayuan Ding, Christopher Xu, Yuying Xie, and Jiliang Tang. [n. d.]. Bi-channel Masked Graph Autoencoders for Spatially Resolved Single-cell Transcriptomics Data Imputation. In *NeurIPS 2022 AI for Science: Progress and Promises*.
- [85] Cameron G Williams, Hyun Jae Lee, Takahiro Asatsuma, Roser Vento-Tormo, and Ashraful Haque. 2022. An introduction to spatial transcriptomics for biomedical research. *Genome Medicine* 14, 1 (2022), 1–18.
- [86] Kan Wu, Houwen Peng, Minghao Chen, Jianlong Fu, and Hongyang Chao. 2021. Rethinking and improving relative position encoding for vision transformer. In *Proceedings of the IEEE/CVF International Conference on Computer Vision*. 10033–10041.
- [87] Mingxing Xu, Wenrui Dai, Chunmiao Liu, Xing Gao, Weiyao Lin, Guo-Jun Qi, and Hongkai Xiong. 2020. Spatial-temporal transformer networks for traffic flow forecasting. *arXiv preprint arXiv:2001.02908* (2020).
- [88] Dong Zhang, Hanwang Zhang, Jinhui Tang, Meng Wang, Xiansheng Hua, and Qianru Sun. 2020. Feature pyramid transformer. In *Computer Vision–ECCV 2020: 16th European Conference, Glasgow, UK, August 23–28, 2020, Proceedings, Part XXVIII 16*. Springer, 323–339.

## A DATA AVAILABILITY

Two datasets (Lung and Liver) we used are public available on Nanostring official website: <https://nanostring.com/products/cosmx-spatial-molecular-imager/nsclc-ffpe-dataset/>.

## B CODE AVAILABILITY

Our codes for reproducibility are released on GitHub: <https://github.com/wehos/CellT>.